Structure of the martian wake

A. Fedorov [a,*], E. Budnik [a], J.-A. Sauvaud [a], C. Mazelle [a], S. Barabash [b], R. Lundin [b], M. Acuña [c], M. Holmström [b], A. Grigoriev [b], M. Yamauchi [b], H. Andersson [b], J.-J. Thocaven [a], D. Winningham [d], R. Frahm [d], J.R. Sharber [d], J. Scherrer [d], A.J. Coates [i], D.R. Linder [i], D.O. Kataria [i], E. Kallio [e], H. Koskinen [e], T. Säles [e], P. Riihelä [e], W. Schmidt [e], J. Kozyra [f], J. Luhmann [g], E. Roelof [h], D. Williams [h], S. Livi [h], C.C. Curtis [j], K.C. Hsieh [j], B.R. Sandel [j], M. Grande [k], M. Carter [k], S. McKenna-Lawler [l], S. Orsini [m], R. Cerulli-Irelli [m], M. Maggi [m], P. Wurz [q], P. Bochsler [q], N. Krupp [n], J. Woch [n], M. Fränz [n], K. Asamura [o], C. Dierker [p]

[a] *Centre d'Etude Spatiale des Rayonnements, BP-4346, F-31028 Toulouse, France*
[b] *Swedish Institute of Space Physics, Box 812, S-98 128, Kiruna, Sweden*
[c] *Goddard Space Flight Center, Greenbelt, MD, USA*
[d] *Southwest Research Institute, San Antonio, TX 7228-0510, USA*
[e] *Finnish Meteorological Institute, Box 503, FIN-00101 Helsinki, Finland*
[f] *Space Physics Research Laboratory, University of Michigan, Ann Arbor, MI, USA*
[g] *Space Science Laboratory, University of California in Berkeley, Berkeley, CA 94720-7450, USA*
[h] *Applied Physics Laboratory, Johns Hopkins University, Laurel, MD 20723-6099, USA*
[i] *Mullard Space Science Laboratory, University College London, Surrey RH5 6NT, UK*
[j] *University of Arizona, Tucson, AZ 85721, USA*
[k] *Rutherford Appleton Laboratory, Chilton, Didcot, Oxfordshire OX11 0QX, UK*
[l] *Space Technology Ltd., National University of Ireland, Maynooth, Co. Kildare, Ireland*
[m] *Istituto di Fisica dello Spazio Interplanetari, I-00133 Rome, Italy*
[n] *Max-Planck-Institut für Aeronomie, D-37191 Katlenburg-Lindau, German*
[o] *Institute of Space and Astronautical Science, 3-1-1 Yoshinodai, Sagamichara, Japan*
[p] *Technical University of Braunschweig, Hans-Sommer-Strasse 66, D-38106 Braunschweig, Germany*
[q] *Physikalisches Institut, University of Bern, CH-3012 Bern, Switzerland*

Abstract

We present the first results from the ion mass analyzer IMA of the ASPERA-3 instrument on-board of Mars Express. More than 200 orbits for May 2004–September 2004 time interval have been selected for the statistical study of the distribution of the atmospheric origin ions in the planetary wake. This study shows that the martian magnetotail consists of two different ion regimes. Planetary origin ions of the first regime form the layer adjacent to the magnetic pile-up boundary. These ions are accelerated to energy greater than 2000 eV and exhibit a gradual decreasing of energy down to the planetary tail. The second plasma regime is observed in the planetary shadow. The heavy ions (considered as planetary ones) are accelerated to the energy of the solar wind protons. Obviously the acceleration mechanism is different for the different plasma regimes. Study of two plasma regimes in the frame referred to the interplanetary magnetic field (IMF) direction (we used MGS magnetometer data to obtain the IMF clock angle) clearly shows their spatial anisotropy. The monoenergetic plasma in the planetary shadow is observed only in the narrow angular sector around the positive direction of the interplanetary electric field.
© 2005 Elsevier Inc. All rights reserved.

Keywords: Mars; Magnetospheres

---

* Corresponding author. Fax: +33 (0) 561 55 67 01.
E-mail address: andrei.fedorov@cesr.fr (A. Fedorov).

1. Introduction

The interaction of the solar wind with the martian atmosphere and ionosphere is an important factor of planetary evolution. Solar wind convecting media can pick-up and accelerate ions of planetary origin. This process results to the irretrievable escape of the atmospheric particles to the space. The mechanism of the solar wind–atmosphere interaction is the complex and interesting physical problem that has being investigated since 1971 when the first soviet missions Mars-2 and Mars-3 have reached the Red Planet (Vaisberg, 1992, and references therein) or even since the theoretical study of Alfvén (1957).

Now, after several "Mars" missions, Phobos-2 measurements (Lundin et al., 1989), NASA MGS findings (Vignes et al., 2000), and numerous numerical simulations (Brecht, 2002; Kallio and Janhunen, 2002; Ma et al., 2002; Lichtenegger and Dubinin, 1998; Sauer and Dubinin, 2000) the general picture of the martian space environment is more or less clear. Fig. 1 shows its common structure. Since the definitions of the regions and boundaries shown in Fig. 1 caused long discussions between investigators, we prefer to give here and use in the present paper the most popular terms after Nagy et al. (2004). The martian ionosphere is an obstacle for the incident flow of the solar wind. In addition an ionization of extended neutral atmosphere results in the significant mass-loading of the frozen-in interplanetary magnetic field (IMF). Draping and pile-up of the solar wind magnetic field at this obstacle and exchange of the solar wind flow to the flow of heavy (mostly O^+ and O_2^+) ions leads to creation of magnetic pile-up boundary (MPB) (Vignes et al., 2000), which separates thermalized solar wind plasma ("magnetosheath" in Fig. 1) from the region filled by ions of planetary

origin. The last one is called magnetic pile-up region (MPR). Note that MPB is transparent for interplanetary magnetic field (IMF) and for the solar wind electrons. MPR manifests itself by relatively weak flow of energized ions of planetary origin. But behind the planet, especially in the planet shadow, the satellite can encounter the dense flow of the heavy ions. This region has been called "plasma sheet" (PS) (Rosenbauer et al., 1989).

Due to a limited volume of the data collected by Phobos-2 mission the plasma morphology of MPR and PS is poorly known. Now we have the possibility to improve significantly our knowledge on martian space environment with more than one year of observations of the ASPERA-3 instrument onboard of Mars Express. The subject of the present paper is to clarify the spatial structure of the martian wake, and the properties of MPR and plasma sheet. It is worth to note here that the ions of planetary origin are accelerated by a convective electric field which is mostly parallel to the electric field of the solar wind. Yet, the movement of these accelerated particles is controlled by the local magnetic field which lies in the plane of the IMF in the wake region. Thus the main plasma processes in the martian wake is referred to $\mathbf{V} \times \mathbf{B}$ direction (Russell et al., 1995; Moore et al., 1990). We use such a frame for the present statistical study. To get $\mathbf{V} \times \mathbf{B}$ direction we used the magnetic measurements of Mars Global Surveyor (MGS).

The paper is organized in a following way. We first present measurements background such as satellite orbit, instrumentation and data base. Then in the third section we show several examples of observations in MPR and PS. The next section is devoted to the results of statistical analysis on the properties of planetary ions. We describe the IMF clock angle extraction technique in Section 6.
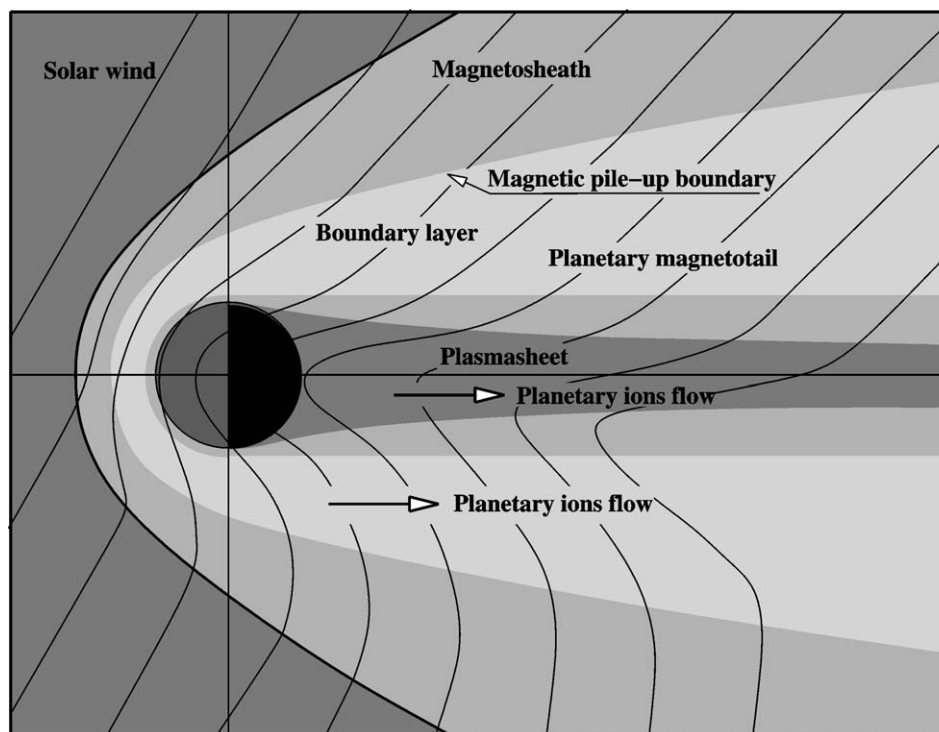

Fig. 1. Structure of the martian plasma environment in the plane of IMF. Adopted from Nagy et al. (2004).

2. Introduction to the measurements

As it was mentioned in the introduction this work was based on the data from the IMA ion mass analyzer which is a part of the ASPERA-3 plasma package. Entire ASPERA-3 package consists of IMA, an electron analyzer, and two neutral atoms detectors. The complete description of the instrument the reader can find in Barabash et al. (2004). Here we just note that the ion analyzer IMA has almost 4π field of view with angular resolution equal to $22° \times 6°$. The $360°$ azimuthal field of view of the sensor is divided into 16 sectors working as parallel measurement channels. The instrument scans over the polar angular range. The energy range of the sensor is 20–30,000 eV/charge. The M/Q region extends from 1 up to infinity. The instrument can resolve solar wind ions H^+ and He^{2+} and planetary origin ions O^+, O_2^+. The heavier ions can be distinguished from O_2^+, but not from each other. Accumulation of one complete angular-energy-mass spectrum takes 192 s. Most of the time the instrument was working in the mode cutting off H^+ with energy less than 1000 eV. Because of that, for the present statistical study, we use He^{2+} ions as an indicator of the solar wind flow in the magnetosheath, especially as there is no such ions in the martian ionosphere. We consider any ions with $M/Q > 12$ as the ions of planetary origin.

In this paper we use two coordinate systems: MSO and MSE. MSO reference frame has Cartesian components as follows: (1) X_{MSO}—toward Sun, Y_{MSO}—opposite to martian velocity vector, Z_{MSO}—completes the right-hand system. (2) MSE frame has $X_{MSE} = X_{MSO}$ but other components are different: Z_{MSE} is parallel to $\mathbf{E} = \frac{1}{c}\mathbf{e}_X \times \mathbf{B}$. Here $\mathbf{e}_X$ is the unit vector parallel to X_{MSO}, and $\mathbf{B}$ is the interplanetary magnetic field (IMF). Y_{MSE} completes the right-hand system. IMF direction has been estimated by MGS data (see Section 6 for details).

Fig. 2 shows an example of spacecraft orbit in MSO coordinate system. All data used in the present paper has been collected during May–August 2004 time interval. At this time a certain part of each orbit was lying antisunward from the planet, and for a relatively short time the spacecraft passed the eclipse. We studied only data collected when X_{MSO} has been negative and $\sqrt{Y_{MSO}^2 + Z_{MSO}^2} < 2.5\ R_M$. Here R_M is the radius of Mars. One can see that orbits cover relatively wide region below MPB down to $X_{MSO} = -1.8\ R_M$. The bow shock and MPB shown as the blue curves, are derived from the analytical equations by Kallio (1996) (assuming that "magnetopause" and MPB is the same boundary, see Lundin and Barabash, 2004)

$$X_{BS} = 0.55 + \frac{2.04}{1.0 + 1.02\cos(\Theta)}\cos(\Theta), \tag{1}$$

$$R_{BS} = \frac{2.04}{1.0 + 1.02\cos(\Theta)}\sin(\Theta), \tag{2}$$

$$X_{MPB} = -0.0992 R_{MPB}^4 - 0.2967 R_{MPB}^2 + 1.2. \tag{3}$$

Here X is X_{MSO}, $R = \sqrt{Y_{MSO}^2 + Z_{MSO}^2}$ and Θ is the solar–zenith angle.
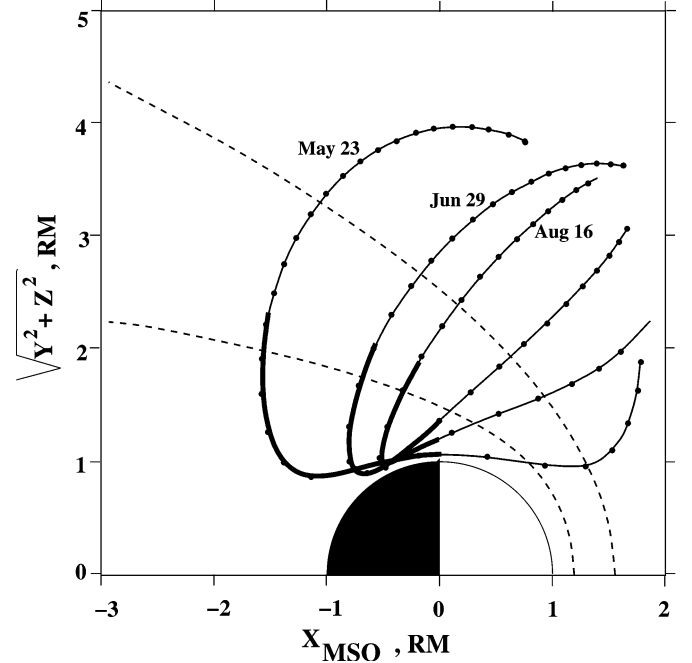

Fig. 2. Several examples of Mars Express orbit in May–August 2004. Each blue tick marks 10 min interval. The parts of the orbits shown in bold are used for the present statistical study. Dashed curves present bow shock and MPB after Kallio (1996) and Lundin and Barabash (2004), correspondingly.

3. Examples of data used for statistical study

Fig. 3 shows a typical example of IMA observations in the wake region. Before 03:11 UT the spacecraft is in the proper magnetosheath. Between 03:11 and 03:15 UT solar wind ions decelerate and disappear. This region corresponds to the mass-loading region introduced by Lundin et al. (1989). Heavy planetary ions replace completely the solar wind flow at 03:15 UT. We identify this transition as magnetic pile-up boundary. The total electron flux drops at the same moment (not shown in the figure). Unfortunately the absence of the magnetic measurements does not allow to prove the identification of this boundary. The pronounced planetary ion flow is seen between 03:15 and 03:25 UT. Note that its energy and intensity decrease with decreasing of $R = \sqrt{Y_{MSO}^2 + Z_{MSO}^2}$. Heavy ions of lower energy are seen until the eclipse at 03:35 UT. It is worth to note that ions with $M/Q = 2$ appear again around 03:25 UT. MGS measurements performed in the same time interval allow to estimate the clock angle ($\arctan(B_{yMSO}/B_{zMSO})$) of the interplanetary magnetic field (IMF). See Section 3 for details. Thus for this case we are able to define the MSE coordinate system. From the right panel of Fig. 3 one can see that interval of intense planetary ion flow lies near the positive direction of the interplanetary electric field (Z_{MSE}).

Fig. 4 shows another case of the wake crossing encountering even more frequently than the previous one. Here the spacecraft crosses MPB at 01:03 UT, but IMA sees nothing until spacecraft enters the planetary shadow. In the MSE frame the region of heavy ions observation lies at the direction of the interplanetary electric field (see the right panel of Fig. 4). The energy of ions is equal to the energy of solar wind protons. Af-
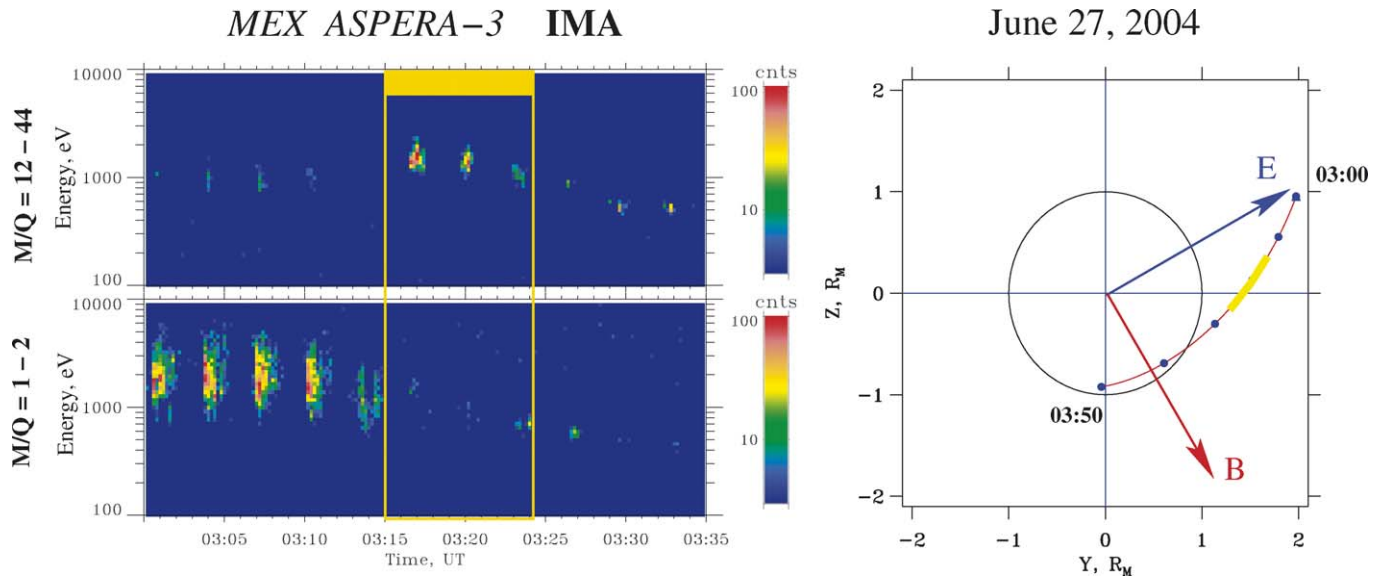
Fig. 3. An example of planetary origin ions observed immediately after crossing of the magnetic pile-up boundary. Right panel shows the spacecraft orbit. Interval of intense planetary ions flow is marked by yellow line. Direction of IMF B_{yz} defines MSE_{yz} frame for this case. Top left panel shows the energy–time spectrogram of heavy ions ($M/Q = 12$–44). The low left panel shows the same for H^+ and He^{2+}. The count range of the sensor is integrated over the azimuthal field-of-view. Modulation of the counts manifests the polar angle scanning.
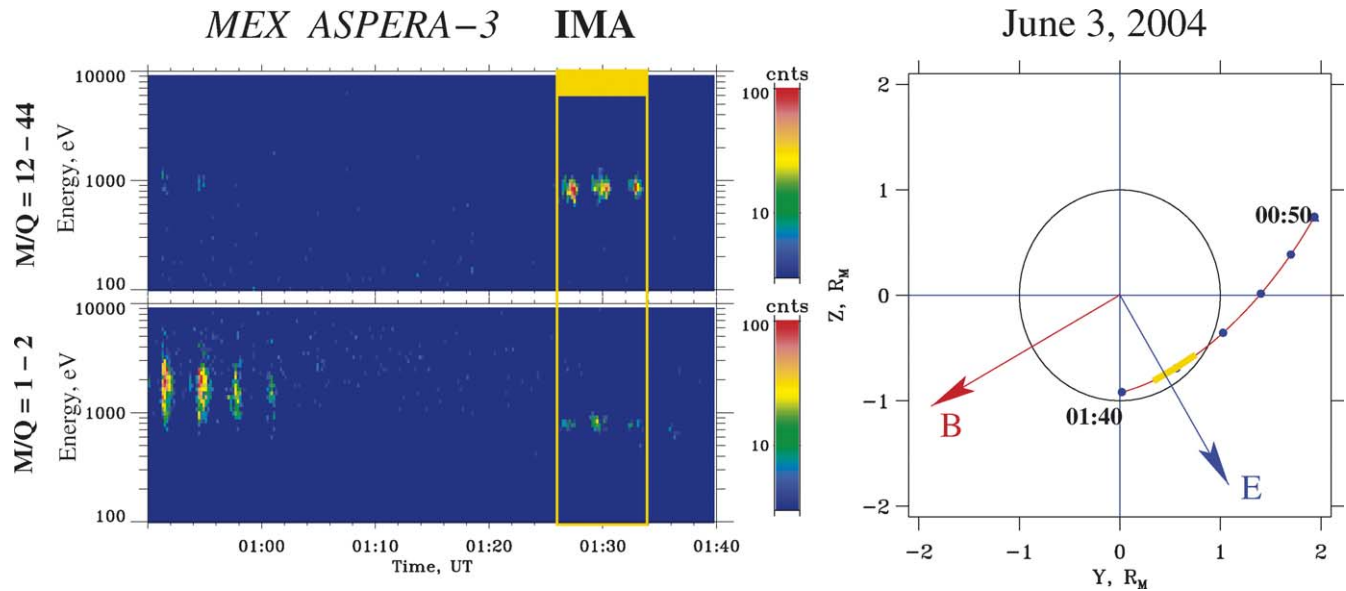

Fig. 4. An example of observation of planetary ions in the plasma sheet. Layout is the same is in Fig. 3.

ter Rosenbauer et al. (1989) we denote this plasma regime as plasma sheet. Note that the weak flow of $M/Q = 2$ ions is observed in the plasma sheet as well.

4. Statistical study of the martian wake

More than 200 orbits from the May 2004–September 2004 time interval have been selected for the statistical study. Selection criterion was just a presence of IMA data. The statistics accumulated from the entire data set is shown in Fig. 5. The present distribution was obtained by epoch superposition in a predefined grid 0.05×0.05 R_M of the X_{MSO}, $\sqrt{Y_{MSO}^2 + Z_{MSO}^2}$ plane. For each complete IMA spectrum (i.e., for about each

3 min) the total count rate C_M corresponding to the selected mass interval has been calculated. The average count in each spatial cell has been defined as C_M/N. Here N is the number of spectra registered in a given cell. To get a proper statistics, only measurements taken inside the cone $\pm 40°$ looking sunward have been taken into account. At the right panel of Fig. 5 one can see that the flow of solar wind ions is practically stopped at the theoretical (Vignes et al., 2000) pile-up boundary. Note that ions with $M/Q = 2$ appear again at the minimal R point.

The ions with $M/Q = 12$–44 of the planetary origin appear only downstream the MPB. The spatial distribution of the heavy ions demonstrates two distinct clusters. One of them is
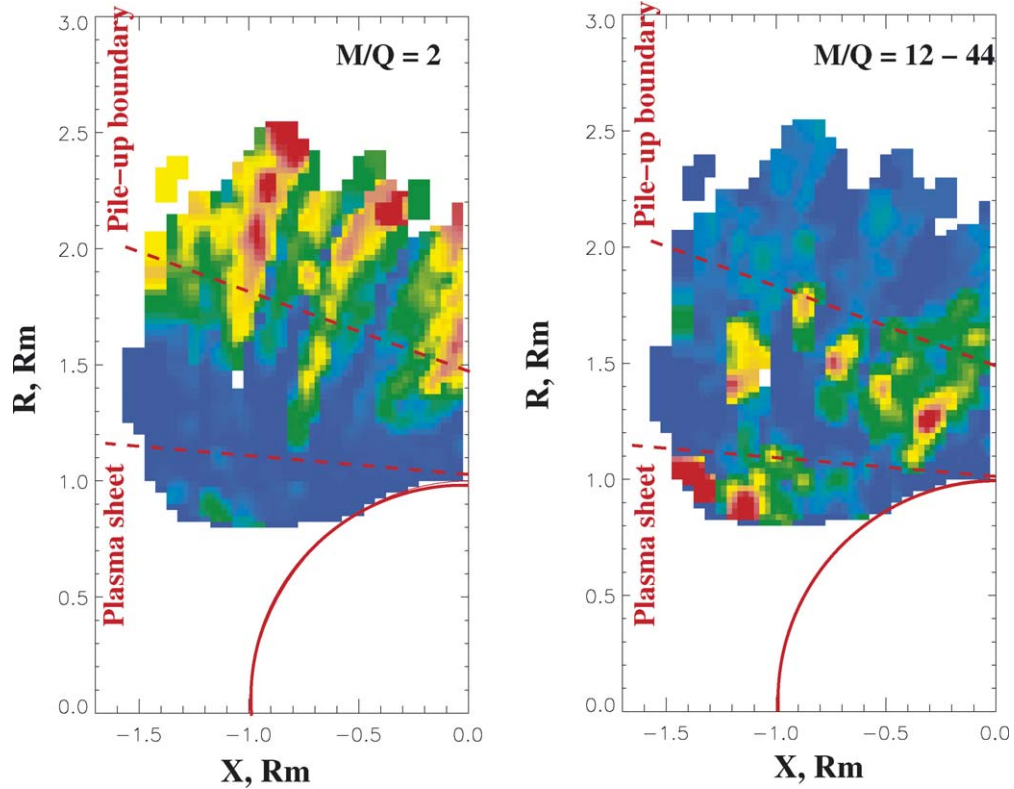
Fig. 5. Spatial distribution of the average IMA count rate for $M/Q = 2$ (left panel) and $M/Q = 12$–44 (right panel). The vertical axis is $\sqrt{Y_{MSO}^2 + Z_{MSO}^2}$. The horizontal axis is X_{MSO}. The pile-up boundary is drawn after Kallio (1996). Plasma sheet boundary position is estimated from the present data. Color codes the particles flow in the arbitrary units. Red corresponds to the maximum flow, blue corresponds to zero flow, and white corresponds to the absens of data in the given point.
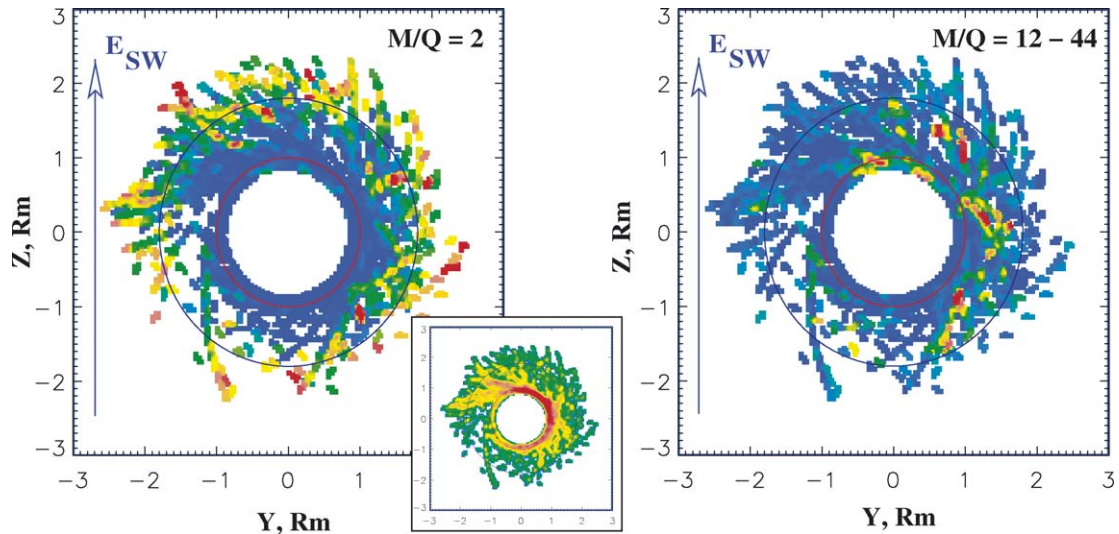

Fig. 6. Spatial distribution of the average IMA count rate presented in the (Y_{MSE}, Z_{MSE}) frame. Left panel shows distribution of $M/Q = 2$. Right panel shows the same for $M/Q = 12$–44. Color code is the same as in Fig. 5. Red circle shows the planet limb and the black one shows the MPB at $X_{MSE} = -1$ R_M. Insert in the center shows the orbital statistics of the presented data. Green color corresponds to the single passage through the given cell, and red color corresponds to 7 passages. Average data in the main panels are normalized to the number of measurements.

located in the magnetic pileup region just outside of the planetary shadow. The second one is placed behind the planet. Later we will show that energy properties of the ions belonging to the second cluster, and their spatial distribution in the MSE frame are quite different from the properties of the first cluster. Now, just preliminary, we call the second cluster as "plasma sheet," and put the PS boundary at the boundary of the planetary shadow.

Fig. 6 shows the same distribution but in (Y_{MSE}, Z_{MSE}) plane. Since we can not define IMF clock angle for arbitrary time, only part of the entire data set is used in the present statistics. One can see that planetary ions are distributed in the

(Y_{MSE}, Z_{MSE}) plane quite asymmetrically. There are two distinct features: (1) The heavy ions in the magnetic pileup region are concentrated at the positive Y_{MSE}. (2) The planetary ions behind the planet (plasma sheet) are placed in the very small region located in the north hemisphere near $Y_{MSE} = 0$. It is worth to note that this distribution is statistically valid. Orbit coverage of the (Y_{MSE}, Z_{MSE}) plane is good enough (blue color) at least in the northern hemisphere and inside the planet shadow.

Scatterplot of the particles energy shown in Fig. 7 provides an additional evidence of the significant difference between plasma regime observed in MPR and the same observed in the planet shadow. Ions energy reaching 2000 keV at MPB gradually decreases down into the magnetosphere. But at $\sqrt{Y_{MSO}^2 + Z_{MSO}^2} \approx 1 R_M$ the ions energy jumps up to the 1 keV, i.e., to the energy of solar wind protons.

5. Discussion and conclusions

Our measurements have confirmed the main features of the martian plasma environment that have been discovered since the first measurements from the space probes. The gradually decreasing of the energy of the planetary ions from MPB down to plasma sheet (see Figs. 3 and 7) was mentioned by Lundin et al. (1991) and then Kallio et al. (1995). The typical feature of the martian tail, that energy of heavy ions in the plasma sheet is about the energy of protons in the solar wind was reported by Dubinin et al. (1993). Rosenbauer et al. (1989) and then Dubinin et al. (1993) mentioned that energy of the planetary ions on the sides of plasma sheet is less than in its center. Many authors (Dubinin et al., 1991; Kallio et al., 1995; Kotova et al., 1997) supposed that the plasma sheet is located in the narrow layer associated with the current sheet in the mar-

tian tail. All these properties of the plasma sheet have been proven by numerical simulation. Lichtenegger et al. (1995) and Lichtenegger and Dubinin (1998) have shown that magnetic shear stress ($\mathbf{J} \times \mathbf{B}$) in the current sheet with finite gyroradius of the ions followed by charge separation leads to the observed ion acceleration. Different types of the ion acceleration in the martian wake have been discussed also by Kotova et al. (1997). The narrow vertical plasma sheet is well seen, for instance, in
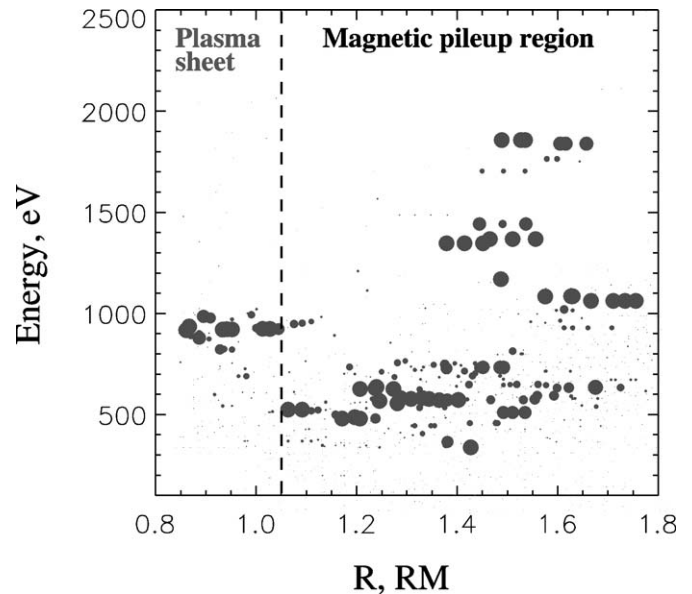

Fig. 7. Scatterplot of the planetary ions energy versus $\sqrt{Y_{MSO}^2 + Z_{MSO}^2}$. Each circle corresponds to the one complete IMA energy–angular spectrum. The diameter of the circle shows the total count rate of the event. The vertical dashed line separates MPR from the plasmasheet.
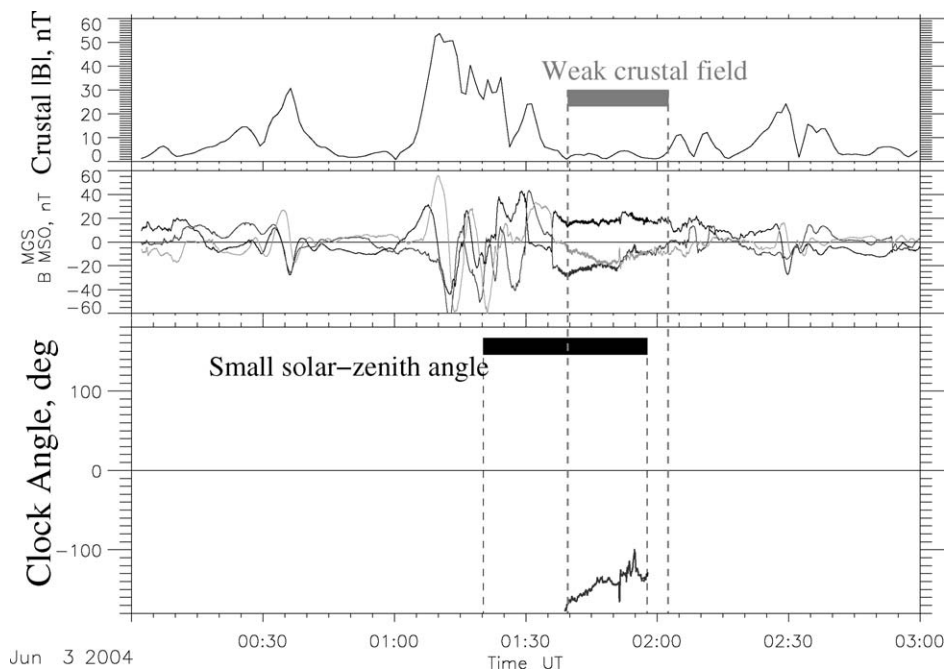

Fig. 8. Top panel: Magnitude of the crustal magnetic field along the MGS orbit calculated by Cain's model (Cain et al., 2003). Middle panel: MGS magnetometer measurements, black profile represents B_{xMSO}, light gray and dark gray ones represent B_{yMSO} and B_{zMSO} correspondingly. Low panel shows the IMF clock angle calculated for selected time interval. See details in the text.
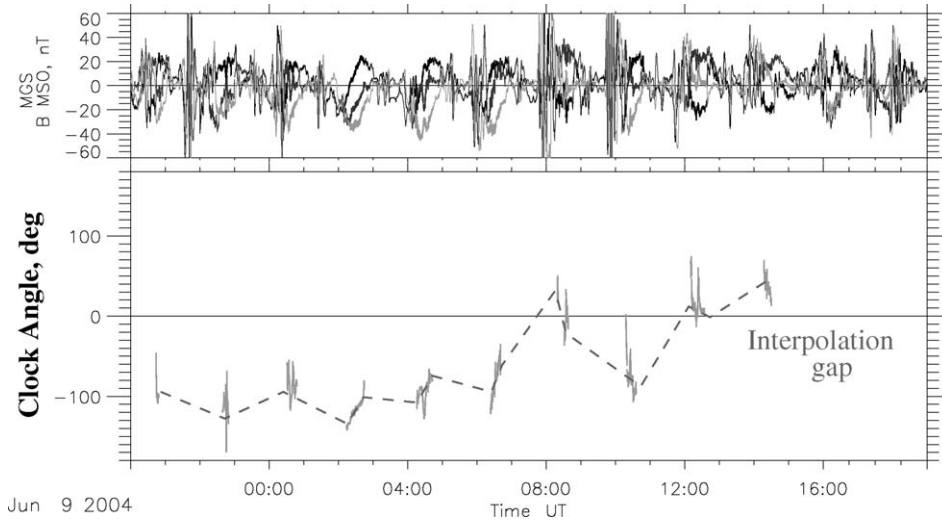
Fig. 9. Top panel: The same as middle panel in Fig. 8. Low panel shows the IMF clock angle (Φ) calculated only for short time intervals and interpolated if possible (dashed line). See details in the text.

the Modolo et al. (2005) simulations. But statistics provided by Kallio et al. (1995) and Dubinin et al. (1996) do not show really narrow vertically organized plasma sheet. Probably it is result of relatively poor statistics.

In addition to the previous publications (but not in contrast to them), the present paper claims that the martian wake consists of two rather different plasma regimes: (1) Ions of planetary origin, observed in the magnetic pileup region, are concentrated mostly at the positive side of Y_{MSE} (Fig. 6). The energy of these ions drops down with decreasing of $\sqrt{Y_{MSO}^2 + Z_{MSO}^2}$ (Fig. 7). (2) Plasma sheet ions of planetary origin, observed in the narrow region located around $Y_{MSE} = 0$, at the positive side of Z_{MSE} (see Fig. 6). The energy of plasma sheet ions is always close to the energy of solar wind protons. Moreover, the spatial boundary between these two regimes is sharp and manifests itself by energy step (see Fig. 7). Kallio et al. (2006) shows that the plasma sheet ions observed on June 3, 2004 (Fig. 4) are associated with the kink on the draped magnetic field, i.e., with the current sheet.

In our statistics the current sheet is never seen at $Y_{MSE} < -0.7\ R_M$ and $Y_{MSE} > 0.7\ R_M$. Also we can definitely say that at $Z_{MSE} \approx -1\ R_M$ plasma sheet does not exist. This result deviates from the previous statistics, but it is well consistent with the numerical simulation by Modolo et al. (2005). Unfortunately at the moment there is no measurements of IMA in the deep martian eclipse. Another important issue is coming from the narrow distribution of the plasma sheet ions: they cannot be related to the martian magnetic anomalies. Their strong clusterization in MSE coordinate system shows that only IMF (or mainly IMF) controls plasma sheet generation.

It is difficult to explain Y_{MSE} asymmetry of the ions registered in the MPR. One can assume that this feature can be related to the Parker spiral. Due to the significant B_x component of IMF, the draping pattern of the magnetic field lines behind the planet has a left–right asymmetry, which can lead to the appropriate effects. But this problem is left to the future work. Also the property of the ions of the different species in

the wake, and detailed investigations of the role of the magnetic anomalies in the plasma acceleration are the subjects of the future studies.

6. Annex: IMF clock angle determination

IMF clock angle has been defined from Mars Global Surveyor (MGS) data as follows: (1) Only parts of orbits with solar–zenith angle less than 60° were taken into account. Such time interval is marked by black rectangle in Fig. 8. (2) Only parts of the orbit where Cain's model (Cain et al., 2003) predicts the magnitude of the crustal magnetic field less than 3 nT were taken into account. This time interval is marked by gray rectangle in Fig. 8. (3) Time intervals where conditions (1) and (2) are true are chosen for the IMF clock angle calculation

$$\Phi = \arctan(B_{zMSO}/B_{yMSO}). \qquad (4)$$

Fig. 9 shows 24 h of MGS observations. One can see that Φ can be calculated only for very short time intervals. If the lag between two Φ measurements is less than 2.5 h, the empty interval is linearly interpolated. If not, the data gap is registered.

References

Alfvén, H., 1957. On the theory of comet tails. Tellus 18, 92–96.

Barabash, S., Lundin, R., Andersson, H., Gimholt, J., Holmström, M., Norberg, O., Yamauchi, M., Asamura, K., Coates, A.J., Linder, D.R., Kataria, D.O., Curtis, C.C., Hsieh, K.C., Sandel, B.R., Fedorov, A., Grigoriev, A., Budnik, E., Grande, M., Carter, M., Reading, D.H., Koskinen, H., Kallio, E., Riihela, P., Säles, T., Kozyra, J., Krupp, N., Livi, S., Woch, J., Luhmann, J., McKenna-Lawlor, S., Orsini, S., Cerulli-Irelli, R., Mura, A., Milillo, A., Roelof, E., Williams, D., Sauvaud, J.-A., Thocaven, J.-J., Winningham, D., Frahm, R., Scherrer, J., Sharber, J., Wurz, P., Bochsler, P., 2004. The Analyzer of Space Plasmas and Energetic Atoms (ASPERA-3) for the European Mars Express Mission, ESA Publication SP-1240. ESA Publications Division, Noordwijk, pp. 121–139.

Brecht, S.H., 2002. Numerical techniques associated with simulations of the solar wind interaction with non-magnetized bodies. In: Mendillo, M., Nagy, A., Waite, H. (Eds.), Comparative Aeronomy in the Solar System. AGU, Washington. 141 pp.

Cain, J., Ferguson, B.B., Mozzoni, D., 2003. An $n = 90$ internal potential function of the martian crustal magnetic field. J. Geophys. Res. 108. 2-1.

Dubinin, E., Lundin, R., Riedler, W., Schwingenschuh, K., Luhmann, J.G., 1991. Comparison of observed plasma and magnetic field structures in the wakes of Mars and Venus. J. Geophys. Res. 96, 11189–11197.

Dubinin, E., Lundin, R., Norberg, O., Pissarenko, N., 1993. Ion acceleration in the martian tail: PHOBOS observations. J. Geophys. Res. 98, 3991–3997.

Dubinin, E., Sauer, K., Lundin, R., Norberg, O., Trotignon, J.-G., Schwingenschuh, K., Delva, M., Riedler, W., 1996. Plasma characteristics of the boundary layer in the martian magnetosphere. J. Geophys. Res. 101, 27061–27075.

Kallio, E., Koskinen, H., Barabash, S., Nairn, C.M.C., Schwingenschuh, K., 1995. Oxygen outflow in the martian magnetotail. Geophys. Res. Lett. 22, 2449–2452.

Kallio, E., 1996. An empirical model of the solar wind flow around Mars. J. Geophys. Res. 101, 11133–11147.

Kallio, E., Janhunen, P., 2002. Ion escape from Mars in a quasi-neutral hybrid model. J. Geophys. Res. 107, doi:10.1029/2001JA000090. 1035.

Kallio, E., and 46 colleagues, 2006. Ion escape at Mars: Comparison of a 3-D hybrid simulation with Mars Express IMA/ASPERA-3 measurements. Icarus 182, 350–359.

Kotova, G.A., Verigin, M.I., Shutte, N.M., Remizov, A.P., Rosenbauer, H., Riedler, W., Schwingenschuh, K., Delva, M., Szegö, K., Tatrallyay, M., 1997. Planetary heavy ions in the magnetotail of Mars—Results of the TAUS and MAGMA experiments aboard PHOBOS. Adv. Space Res. 20, 173–176.

Lichtenegger, H., Schwingenschuh, K., Dubinin, E., Lundin, R., 1995. Particle simulation in the martian magnetotail. J. Geophys. Res. 100, 21659–21667.

Lichtenegger, H., Dubinin, E., 1998. Model calculations of the planetary ion distribution in the martian tail. Earth Planets Space 50, 445–452.

Lundin, R., Zakharov, A., Pellinen, R., Borg, H., Huldquist, B., Pissarenko, N., Dubinin, E., Barabash, S., Liede, I., Koskinen, H., 1989. First measurements of the ionospheric plasma escape from Mars. Nature 341 (6243), 609–612.

Lundin, R., Norberg, O., Dubinin, E.M., Pisarenko, N., Koskinen, H., 1991. On the momentum transfer of the solar wind to the martian topside ionosphere. Geophys. Res. Lett. 18, 1059–1062.

Lundin, R., Barabash, S., 2004. The wakes and magnetotails of Mars and Venus. Adv. Space Res. 33, 1945–1955.

Ma, Y., Nagy, A.F., Hansen, K.C., DeZeeuw, D.L., Gombosi, T.I., 2002. Three-dimensional multispecies MHD studies of the solar wind interaction with Mars in the presence of crustal fields. J. Geophys. Res. 107, doi:10.1029/2002JA009293. 1282.

Modolo, R., Chanteur, G.M., Dubinin, E., Matthews, A.P., 2005. Influence of the solar EUV flux on the martian plasma environment. Ann. Geophys. 23, 433–444.

Moore, K.R., McComas, D.J., Russell, C.T., Mihalov, J.D., 1990. A statistical study of ions and magnetic fields in the Venus magnetotail. J. Geophys. Res. 95, 12005–12018.

Nagy, A.F., Winterhalter, D., Sauer, K., Cravens, T.E., Brecht, S., Mazelle, C., Crider, D., Kallio, E., Zakharov, A., Dubinin, E., Verigin, M., Kotova, G., Azxford, W.I., Bertucci, C., Trotignon, J.G., 2004. The plasma environment of Mars. Space Sci. Rev. 111, 33–114.

Sauer, K., Dubinin, E., 2000. The nature of the martian "Obstacle Boundary." Adv. Space Res. 26, 1633–1637.

Rosenbauer, H., Shutte, N., Galeev, A., Gringauz, K., Aptáhy, I., 1989. Ions of martian origin and plasma sheet in the martian magnetosphere—Initial results of the TAUS experiment. Nature 341, 612–614.

Russell, C.T., Mulligan, T., Delva, M., Zhang, T.L., Schwingenschuh, K., 1995. A simple test of the induced nature of the martian tail. Adv. Space Res. 16, (6)69–(6)73.

Vaisberg, O.L., 1992. The solar wind interaction with Mars: A review of results from previous Soviet missions to Mars. Adv. Space Res. 12, 137–161.

Vignes, D., Mazelle, C., Réme, H., Acuña, M.H., Connerney, J.E.P., Lin, R.P., Mitchell, D.L., Clotier, P.A., Crider, D.H., Nes, N.F., 2000. The solar wind interaction with Mars: Locations and shapes of the bow shock and magnetic pile-up boundary from the observations of the MAG/ER experiment on board Mars Global Surveyor. Geophys. Res. Lett. 27, 49–52.